







Article

New Aspects of the Synthesis of *closo*-Dodecaborate Nitrilium Derivatives $[B_{12}H_{11}NCR]^-$ ($R = n-C_3H_7, i-C_3H_7, 4-C_6H_4CH_3, 1-C_{10}H_7$): Experimental and Theoretical Studies

Alexey V. Nelyubin ¹, Ilya N. Klyukin ¹, Alexander S. Novikov ^{2,3}, Andrey P. Zhdanov ¹,
Nikita A. Selivanov ¹, Alexander Yu. Bykov ¹, Alexey S. Kubasov ¹, Konstantin Yu. Zhizhin ^{1,*}
and Nikolay T. Kuznetsov ¹

¹ Kurnakov Institute of General and Inorganic Chemistry, Russian Academy of Sciences, Leninskii pr. 31, 119991 Moscow, Russia

² Institute of Chemistry, Saint Petersburg State University, Universitetskaya Nab. 7-9, 199034 Saint Petersburg, Russia

³ Research Institute of Chemistry, Peoples' Friendship University of Russia (RUDN University), Miklukho-Maklaya St. 6, 117198 Moscow, Russia

* Correspondence: zhizhin@igic.ras.ru; Tel.: +7-926-727-0139

Abstract: The preparation of novel nitrilium derivatives of *closo*-dodecaborate anion $[B_{12}H_{11}NCR]^-$, $R = n-C_3H_7, i-C_3H_7, 4-C_6H_4CH_3, 1-C_{10}H_7$ is described. Target compounds were obtained in good yields (up to 73%). The synthesis of target borylated nitrilium derivatives was characterised by the simplicity of the chemical apparatus and the absence of the necessity for the purification of desired compounds. The crystal structures of previously obtained $[B_{12}H_{11}NCC_3H_7]^-$ and novel $[B_{12}H_{11}NCC_3H_7]^-$ were established with the help of X-ray structure analysis. DFT-analysis of several nitrilium derivatives $[B_{12}H_{11}NCR]^-$, $R = CH_3, C_3H_7, 4-CH_3C_6H_4$ was carried out. The main peculiarities of the $C\equiv N$ bond of the *exo*-polyhedral substituent were revealed in terms of bond lengths, bond orders and atomic charges. The LUMO orbitals of the systems considered were examined for understanding of the electrophilic nature of the nitrilium derivatives of the *closo*-dodecaborate anion.

Keywords: nitrilium derivative; *closo*-dodecaborate; crystal structure; DFT; bond order; LUMO; Hirshfeld surface analysis



Citation: Nelyubin, A.V.; Klyukin, I.N.; Novikov, A.S.; Zhdanov, A.P.; Selivanov, N.A.; Bykov, A.Y.; Kubasov, A.S.; Zhizhin, K.Y.; Kuznetsov, N.T. New Aspects of the Synthesis of *closo*-Dodecaborate Nitrilium Derivatives $[B_{12}H_{11}NCR]^-$ ($R = n-C_3H_7, i-C_3H_7, 4-C_6H_4CH_3, 1-C_{10}H_7$): Experimental and Theoretical Studies. *Inorganics* **2022**, *10*, 196. <https://doi.org/10.3390/inorganics10110196>

Academic Editor: Marina Yu. Stogniy

Received: 11 October 2022

Accepted: 31 October 2022

Published: 2 November 2022

Publisher's Note: MDPI stays neutral with regard to jurisdictional claims in published maps and institutional affiliations.



Copyright: © 2022 by the authors. Licensee MDPI, Basel, Switzerland. This article is an open access article distributed under the terms and conditions of the Creative Commons Attribution (CC BY) license (<https://creativecommons.org/licenses/by/4.0/>).

1. Introduction

The *closo*-dodecaborate anion $[B_{12}H_{12}]^{2-}$ is one of the most important chemical species among boron cluster compounds [1,2]. This anion, as well as other *closo*-borates $[B_nH_n]^{2-}$, has a number of remarkable properties, such as high thermal and chemical stability, and low toxicity [3–5]. Furthermore, *closo*-borate anions and their derivatives have many potential applications in the design of catalytic systems [6–8], coordination compounds [9–11], solid electrolytes [12–15] etc. The main application of boron cluster compounds, however, is in medical research [16–21]. In addition, to the preparation of potential drugs for Boron Neutron Capture Therapy (BNCT), intensive work has been carried out to investigate the antiviral and antimicrobial properties of cluster-containing systems [22].

Derivatives of *closo*-borate anions with *exo*-polyhedral B-N bonds are the most interesting, and most often studied, boron cluster compounds [23–25]. Initially, most interest was focused on ammonium derivatives of *closo*-borate systems $[B_nH_{n-1}NH_3]^-$ [26]. These compounds can be easily modified by substituting the hydrogen atom of the NH_3 -group. Various borylated alkylamines [2,27], amides [21,28], imines [29] and amidines [30] can be prepared by such methods.

Nitrilium derivatives are another important class of cluster systems with *exo*-polyhedral B-N bonds. Nitrilium derivatives of boron clusters contain a polarised $N\equiv C$ bond and

have similar chemical properties to transition metal complex compounds, with nitrile ligands [31–33]. Nitrilium derivatives readily enter nucleophilic addition reactions. This peculiarity enables nitrilium derivatives to be applied as a starting point for obtaining different borylated systems. Various borylated imine amides, iminols, imidates, amidines, including those based on amino acids, and oligopeptides have been obtained on the basis of nitrilium derivatives [34,35].

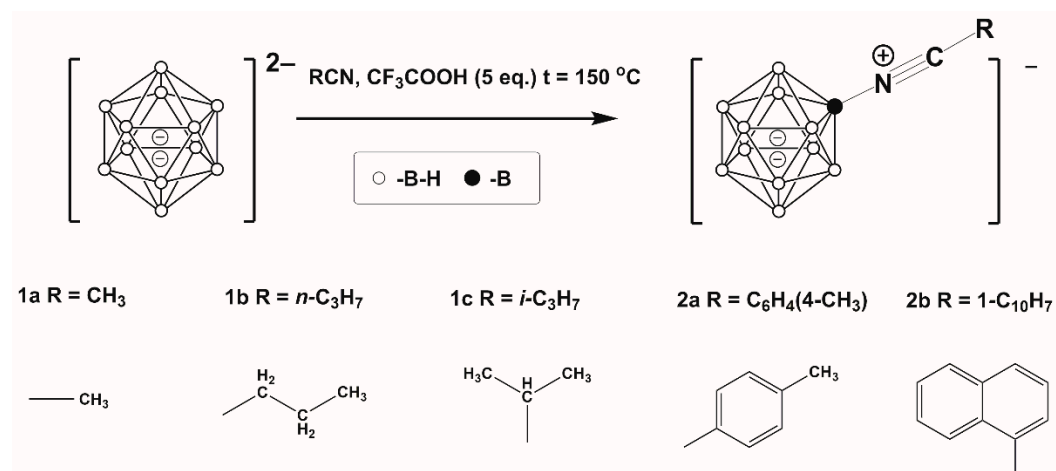
Nitrilium derivatives have been obtained for *closo*-decaborate [36–40], cobalt bisdicarbolyde [41–44] and *nido*-carborane systems [45–48]. Several approaches to the preparation of these systems have been established. All these approaches are based on electrophile-induced nucleophilic substitution [31,49,50]. Several electrophilic inducers were used: CF_3COOH , $\text{CF}_3\text{SO}_3\text{H}$, HgCl_2 and AlCl_3 [51]. Depending on reaction conditions and inducer nature, mono- or dinitrilium derivatives of cluster systems can be obtained.

In several works, nitrilium derivatives of *closo*-dodecaborate anions were prepared $[\text{B}_{12}\text{H}_{11}\text{NCR}]^-$, $\text{R} = \text{CH}_3$, CH_2CH_3 [40,52] and different reaction protocols were applied. In paper [52], the most optimal method was established. This method was based on obtaining the target substances in a glass autoclave at an oil bath temperature above 150°C . The CF_3COOH was used as an electrophilic inducer. In the present work, this approach was extended to obtaining nitrile complexes $[\text{B}_{12}\text{H}_{11}\text{NCR}]^-$, $\text{R} = n\text{-C}_3\text{H}_7$, $i\text{-C}_3\text{H}_7$, $4\text{-C}_6\text{H}_4\text{CH}_3$, $1\text{-C}_{10}\text{H}_7$. The main goal of the current research was to establish the best conditions for the obtaining derivatives, with both aliphatic and aromatic substituents. In addition, theoretical investigation was devoted to the impact of boron clusters on the $\text{N}\equiv\text{C}$ bond nature in target derivatives.

2. Results

2.1. Synthesis of *closo*-Dodecaborate Nitrilium Derivatives

As previously stated, the main goal of the present research was to establish the best conditions for the preparation of derivatives with both aliphatic and aromatic substituents. The approach used was one that had been employed by the authors in previous research [52]. This process involved obtaining the target substances in a glass autoclave at an oil bath temperature above 150°C . The CF_3COOH was used as an electrophilic inducer (Scheme 1). As in the case of the acetonitrile derivative, the complete conversion of the initial salt of *closo*-dodecaborate anion with tetrabutylammonium cations $((n\text{-C}_4\text{H}_9)_4\text{N})^+$ occurred in about 30 min. Increasing the reaction time had a negative effect on the yield of the target nitrile derivative due to formation of additional by-products such as carboxylic derivatives of *closo*-dodecaborate anion.



Scheme 1. Scheme of preparation of $[\text{B}_{12}\text{H}_{11}\text{NCR}]^-$.

The completeness of the reaction was monitored using ^{11}B NMR. As in the case of $[\text{B}_{12}\text{H}_{11}\text{NCCH}_3]^-$, there were two signals observed in the spectra of the target compounds.

A signal from the substituted boron atom lay in the range -12.0 – -12.3 ppm; the signal from unsubstituted boron atoms B(2-12) lay in the range -14.5 – -15.2 .

The yields of nitriles $[\text{B}_{12}\text{H}_{11}\text{NCR}]^-$ obtained were in the range of 69–73%, in all cases except $[\text{B}_{12}\text{H}_{11}\text{NCR}]^-$, $\text{R} = \text{C}_{10}\text{H}_7$ (yield = 36%). These values were lower than in the case of $[\text{B}_{12}\text{H}_{11}\text{NCCH}_3]^-$, relating to the increasing solubility of $[\text{B}_{12}\text{H}_{11}\text{NCR}]^-$ in the mixture of $\text{CH}_3\text{COOH}/\text{CF}_3\text{COOH}$, (this mixture was used for washing nitrilium products). In case of $[\text{B}_{12}\text{H}_{11}\text{NCR}]^-$, $\text{R} = \text{C}_{10}\text{H}_7$ the low yields is additionally related to the reduced nucleophilic capacity of $\text{C}_7\text{H}_{10}\text{CN}$ compared with other nitriles. The yields of the target products were at an acceptable level and losses of target products were compensated by the ease of their isolation.

Apart from $^{11}\text{B}\{\text{H}\}$ NMR, the target *closo*-dodecaborate derivatives were characterised using ^1H and $^{13}\text{C}\{\text{H}\}$ NMR, IR and ESI MS methods. In ^1H NMR spectra, signals from the tetrabutylammonium cation and a signal from the side R group of nitrilium derivatives were observed.

In $^{13}\text{C}\{\text{H}\}$ NMR spectra, tetrabutylammonium cation signals were observed at 59.4, 24.4, 20.2 and 13.9 ppm for $(\text{N}(n\text{-C}_4\text{H}_9)_4)^+$. Signals from carbon atoms of the nitrilium group were in the interval 115.5–103.3 ppm in the case of nitrilium derivatives with aliphatic backbones $\text{R} = n\text{-C}_3\text{H}_7$, *i*- C_3H_7 . These values were more positive than with $[\text{B}_{12}\text{H}_{11}\text{NCCH}_3]^-$. In the case of borylated nitriles with aromatic backbones $\text{R} = 1\text{-C}_{10}\text{H}_7$, 4- $\text{C}_6\text{H}_4\text{CH}_3$, signals from carbon atoms of the nitrilium group were in the interval 103.3–104.2 ppm.

In the IR-spectra of $[\text{B}_{12}\text{H}_{11}\text{NCR}]^-$, $\text{R} = n\text{-C}_3\text{H}_7$, *i*- C_3H_7 , 4- $\text{C}_6\text{H}_4\text{CH}_3$, 1- C_{10}H_7 there were the two most significant absorption bands: from BH valence vibrations in the range 2490 – 2500 cm^{-1} and from CN valence vibrations in the range 2304 – 2338 cm^{-1} .

The target derivatives can be obtained without complex purification procedures. All derivatives obtained are stable in air and can be stored without specific conditions (such as an argon atmosphere or a vacuum). Over time, these compounds experience no more than slight hydrolysis processes of the nitrile group. These circumstances are additional advantages of utilising $[\text{B}_{12}\text{H}_{11}\text{NCR}]^-$ as potential molecular species for various applications.

2.2. X-ray Analysis

The crystals for X-ray diffraction experiments were obtained by isothermal evaporation of acetonitrile solutions of the corresponding derivative, in the presence of $(\text{C}_2\text{H}_5)_4\text{NCl}$ in case of $[\text{B}_{12}\text{H}_{11}\text{NCCH}_3]^-$ and $(\text{C}_6\text{H}_5)_4\text{PCl}$ in case of $[\text{B}_{12}\text{H}_{11}\text{NCC}_3\text{H}_7]^-$. The crystallographically independent part of the orthorhombic unit cell (space group Pbcn) of $((\text{C}_2\text{H}_5)_4\text{N})[\text{B}_{12}\text{H}_{11}\text{NCCH}_3]$ salt contained the anion $[\text{B}_{12}\text{H}_{11}\text{NCCH}_3]^-$, which occupied a common position, and two independent halves of the $(\text{C}_2\text{H}_5)_4\text{N}^+$ cation, on the second order axis. The crystallographically independent part of the salt $((\text{C}_6\text{H}_5)_4\text{P})[\text{B}_{12}\text{H}_{11}\text{NC}n\text{-C}_3\text{H}_7]$ triclinic unit cell (P-1) contained one $(\text{C}_6\text{H}_5)_4\text{P}^+$ cation and a $[\text{B}_{12}\text{H}_{11}\text{NC}n\text{-C}_3\text{H}_7]^-$ anion each. The B-N bond length was 1.513(3) Å in compound **1** and 1.514(2) Å in salt **2**; the $\text{C}\equiv\text{N}$ bond lengths were 1.136(3) Å and 1.135(2) Å, respectively. The BNC angles in the compounds deviated slightly from unfolded and were $178.5(3)^\circ$ and $174.4(2)^\circ$, respectively. The average B-N and $\text{C}\equiv\text{N}$ bond lengths in the $[\text{B}_{12}\text{H}_{11}\text{NCR}]^-$ ($\text{R} = \text{CH}_3$, *n*- C_3H_7) anions were 1.514 Å and 1.128 Å (Figure 1).

In the crystal structure of compound **1a**, cation-anion layers of $[\text{B}_{12}\text{H}_{11}\text{NCCH}_3]^-$ anions and $(\text{C}_2\text{H}_5)_4\text{N}^+$ cations were formed, parallel to the plane *ab* (Figure 2a). The anions bound to each other in dimeric pairs by weak $\text{CH} \dots \text{HB}(\text{B})$ contacts were located sequentially above each other along the *a*-axis. The cations and anions were also connected by a network of weak $\text{CH} \dots \text{HB}(\text{B})$ interactions, which are shown as red spots on the Hirschfeld surface of the anion (Figure 2b). $\text{H} \dots \text{H}$ contacts accounted for 92.5% of the anion surface, while $\text{H} \dots \text{C}/\text{C} \dots \text{H}$ and $\text{H} \dots \text{N}/\text{N} \dots \text{H}$ contacts accounted for 5.5% and 2.0% of the anion surface, respectively.

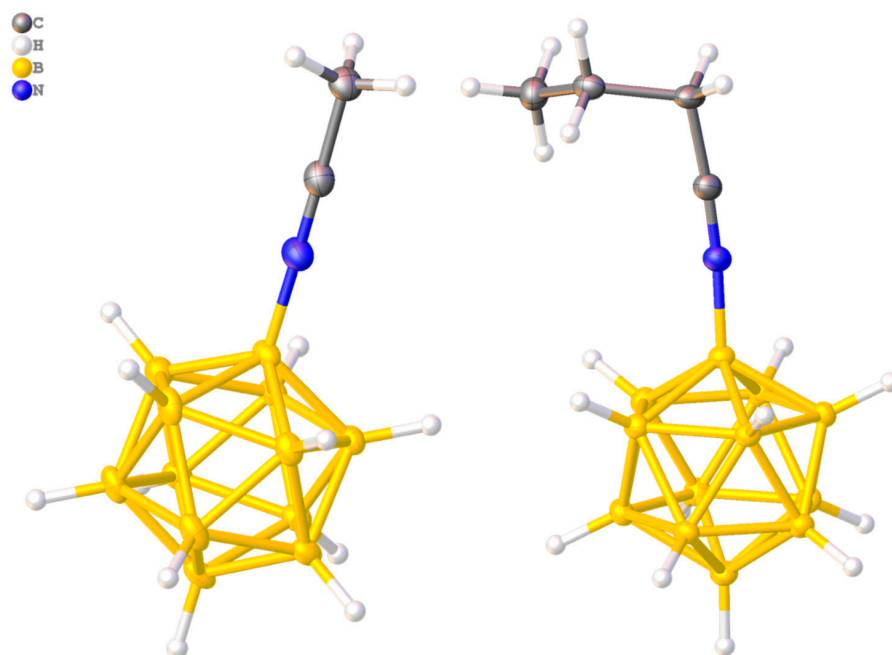


Figure 1. Structures of $[B_{12}H_{11}NCCH_3]^-$ and $[B_{12}H_{11}NCC_3H_7]^-$.

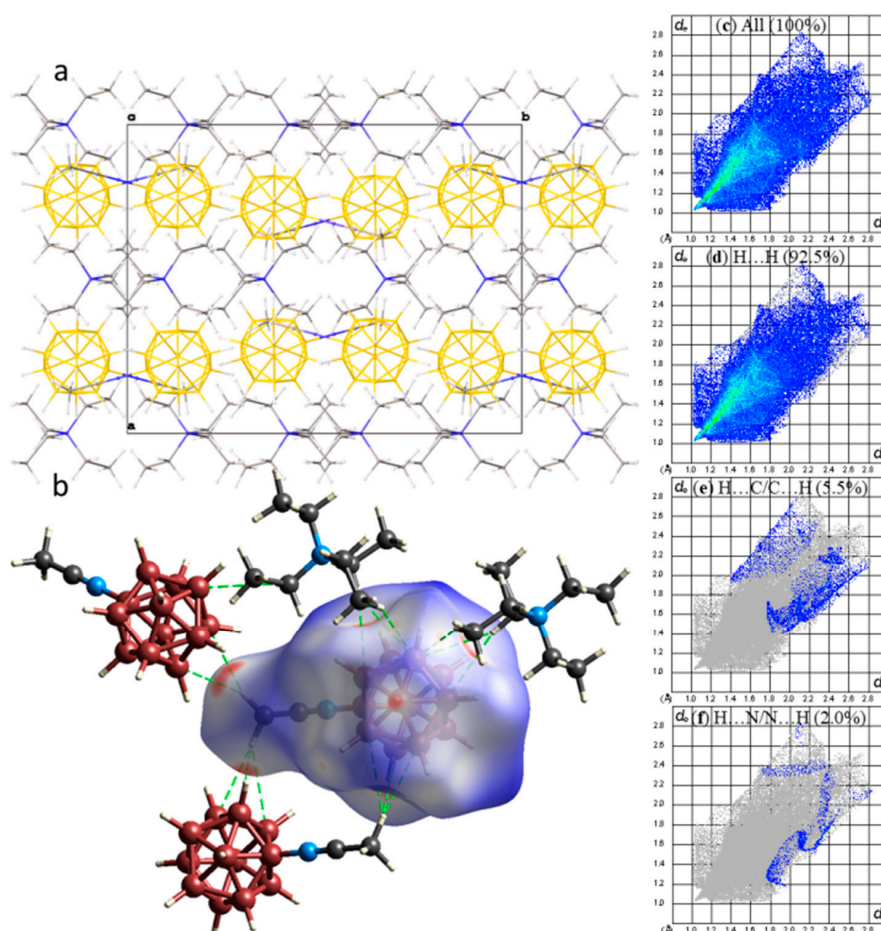


Figure 2. (a) Packing diagram, (b) d_{norm} surface of $((C_2H_5)_4N)[B_{12}H_{11}NCCH_3]^-$ anion, (c) full two-dimensional fingerprint plot for **1a**, together with that delineated into (d) H...H, (e) H...C/C...H, and (f) H...N/N...H contacts.

In the packing of compound **1b**, the picture is similar to that of compound **1a**: the $(C_6H_5)_4P^+$ cations and $[B_{12}H_{11}NCn-C_3H_7]^-$ anions formed cation-anion layers parallel to the *ab* plane, which were bonded together, due to weak $CH \dots HB(B)$ interactions (Figure 3a). The antiparallel $[B_{12}H_{11}NCn-C_3H_7]^-$ anions were similarly bonded by $CH \dots HB(B)$ contacts between the α -methylene groups of the *exo*-polyhedral substituent and the boron backbone of the neighbouring anion (Figure 3b). The Hirshfeld surface fingerprint plot analysis shows that the $H \dots H$ contacts accounted for 88.7% of the anion surface, whereas the $H \dots C/C \dots H$ and $H \dots N/N \dots H$ contacts accounted for 8.9% and 2.3% of the anion surface, respectively.

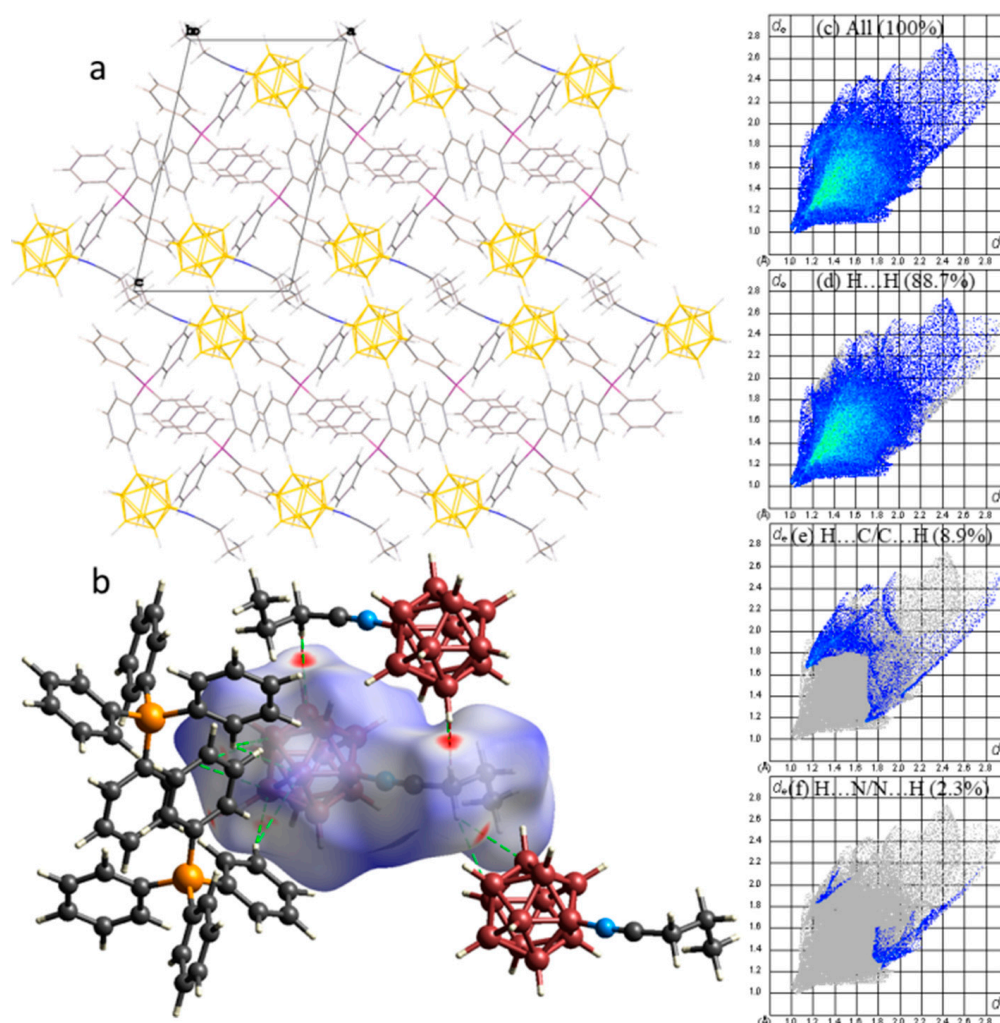


Figure 3. (a) Packing diagram, (b) d_{norm} surface of $((C_6H_5)_4P)[B_{12}H_{11}NCn-C_3H_7]^-$ anion for compound **2**, (c) full two-dimensional fingerprint plot for **2**, together with that delineated into (d) $H \dots H$, (e) $H \dots C/C \dots H$, and (f) $H \dots N/N \dots H$ contacts.

2.3. DFT Calculation

One of the main tasks of the present work was to reveal how the formation of the complex with *closo*-dodecaborate anion affected the properties of the nitrile group. To investigate this phenomenon, several nitriles RCN , $R = CH_3$, $n-C_3H_7$, $4-CH_3C_6H_4$ and nitrilium derivatives $[B_{12}H_{11}NCR]^-$, $R = CH_3$, $n-C_3H_7$, $4-CH_3C_6H_4$ were chosen for theoretical study (Figure 4). All DFT calculations were carried out both in the gas phase and considering solvation effects.

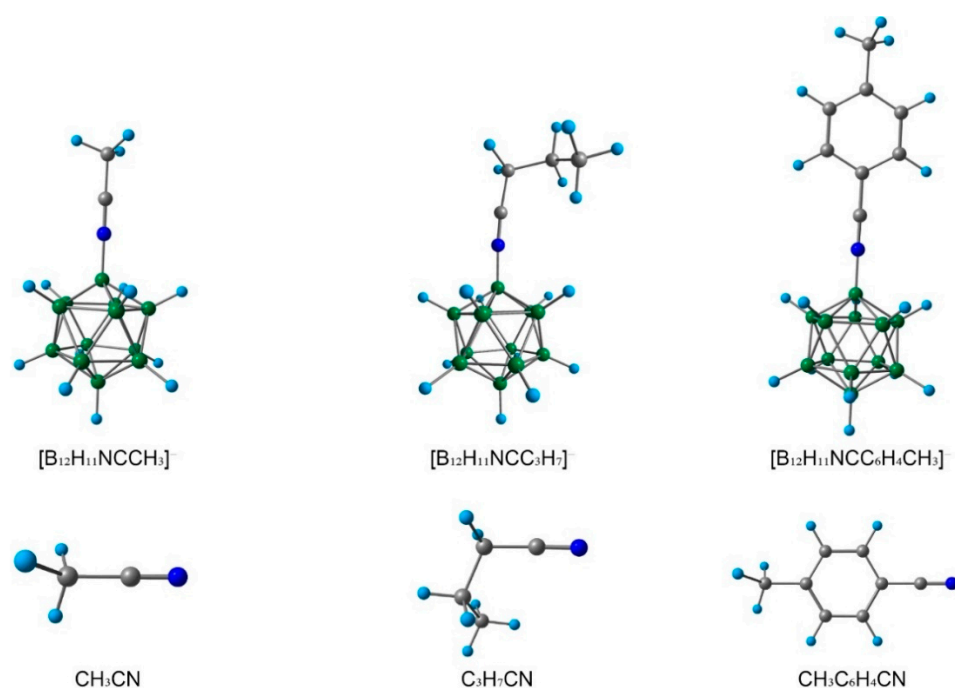


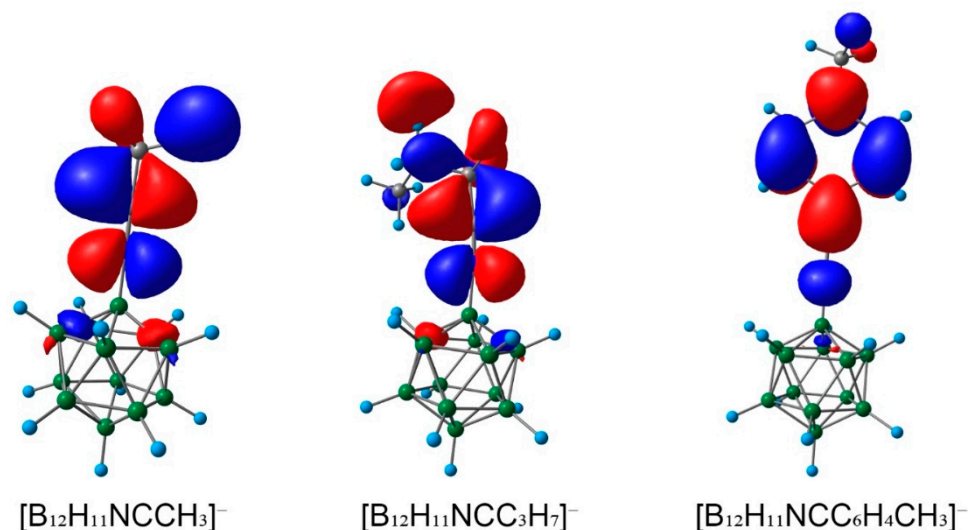
Figure 4. Optimised structure of nitriles RCN, R = CH₃, *n*-C₃H₇, CH₃C₆H₄ and nitrilium derivatives [B₁₂H₁₁NCR]⁺, R = CH₃, *n*-C₃H₇, CH₃C₆H₄.

Firstly, the bond lengths of initial nitriles and borylated complexes were examined (Table 1). It is worth noting that the CN bond lengths were practically the same in the initial nitriles and their borylated analogues. For the estimation of bond orders, the Wiberg and Mayer approaches were used (Table 1). With the Mayer approach, the values of bond orders were higher than with the Wiberg approach. Both Wiberg and Mayer bond orders slightly decreased during the formation of the complex. These changes indicated that the nature of the interaction between nitrogen and carbon atoms had modified. The role of electrostatic interaction between carbon and nitrogen atoms was increased. The carbon atom of the nitrilium group of [B₁₂H₁₁NCR]⁺ became much more positively charged than the initial nitrile. This increase in positive charge also indicated that the carbon atom of the nitrilium group should be much more easily attacked by nucleophile molecules. In the case of CH₃CN and CH₂Cl₂ solutions, mean values of carbon atomic charges were higher than in the gas phase model. The nature of the R-substituent of [B₁₂H₁₁NCR]⁺, R = CH₃, *n*-C₃H₇, 4-CH₃C₆H₄ had a slight effect on the values of the bond lengths and atomic charges.

The increase in electrophilicity can also be correlated with the energy of LUMO (lowest unoccupied orbital). The carbon atom of the nitrilium group makes the largest contribution to LUMO orbitals. As can be seen from the data obtained for the gas phase, the LUMO of [B₁₂H₁₁NCR]⁺ had more positive values of energies than the initial nitriles. When solvation effects were taken into account, the opposite was true. The ratio of LUMO energies explains the much greater reactivity of activated nitriles. This pattern was common to all nitriles considered and their derivatives [B₁₂H₁₁NCR]⁺. The value of LUMO for [B₁₂H₁₁NC(4-C₆H₄CH₃)]⁺ was less positive than for [B₁₂H₁₁NCR]⁺, R = CH₃, *n*-C₃H₇. In addition, the shape of LUMO for [B₁₂H₁₁NC(4-C₆H₄CH₃)]⁺ was quite different to [B₁₂H₁₁NCR]⁺, R = CH₃, *n*-C₃H₇ (Figure 5). In addition to the carbon atom of the nitrilium group, atoms from the benzene ring also made a significant contribution to LUMO.

Table 1. Main considered descriptors of nitriles RCN, R = CH₃, C₃H₇, CH₃C₆H₄ and nitrilium derivatives [B₁₂H₁₁NCR][−], R = CH₃, C₃H₇, CH₃C₆H₄.

Molecular Species	Phase	C≡N Bond Length, Å	Wiberg Bond Index	Mayer Bond Index	C- Charge	LUMO, eV
CH ₃ CN	Gas	1.15	2.91	3.05	0.28	2.85
	CH ₃ CN	1.15	2.88	3.04	0.36	3.22
	CH ₂ Cl ₂	1.15	2.88	3.04	0.35	3.21
[B ₁₂ H ₁₁ NCCH ₃] [−]	Gas	1.14	2.66	2.78	0.50	3.67
	CH ₃ CN	1.14	2.60	2.67	0.66	1.68
	CH ₂ Cl ₂	1.14	2.61	2.69	0.64	1.84
C ₃ H ₇ CN	Gas	1.15	2.92	3.06	0.36	2.53
	CH ₃ CN	1.15	2.88	3.05	0.29	2.85
	CH ₂ Cl ₂	1.15	2.89	3.06	0.35	2.83
[B ₁₂ H ₁₁ NCC ₃ H ₇] [−]	Gas	1.14	2.66	2.76	0.51	3.55
	CH ₃ CN	1.14	2.60	2.68	0.66	1.55
	CH ₂ Cl ₂	1.14	2.61	2.69	0.64	1.72
CH ₃ C ₆ H ₄ CN	Gas	1.15	2.88	3.04	0.28	0.48
	CH ₃ CN	1.15	2.85	3.03	0.35	0.61
	CH ₂ Cl ₂	1.15	2.86	3.03	0.34	0.60
[B ₁₂ H ₁₁ NCC ₆ H ₄ CH ₃] [−]	Gas	1.14	2.62	2.71	0.49	1.51
	CH ₃ CN	1.14	2.57	2.62	0.63	−0.04
	CH ₂ Cl ₂	1.14	2.58	2.64	0.62	0.08

**Figure 5.** LUMO of nitrilium derivatives [B₁₂H₁₁NCR][−], R = CH₃, *n*-C₃H₇, 4-CH₃C₆H₄.

The increased reactivity of borylated nitriles compared with initial nitriles is a well-known and established fact, which can be explained in terms of changes in the nature of the CN chemical bond upon formation of the target complex. In the case of nitrilium derivatives, the CN bond has a more ionic nature than that of initial nitriles. In addition, a change in the energy of the LUMO orbital during the formation of the nitrilium complex also plays a significant role. The decrease in LUMO energy during complex formation provides greater reactivity with nucleophile molecules. These effects are, however, characteristic only when

solvent influence is taken into account. In the gas phase, uncoordinated nitriles have lower positive LUMO values than cluster derivatives.

3. Materials and Methods

3.1. IR Spectra

IR spectra of the compounds were recorded on an Infracalum FT-08 IR Fourier spectrophotometer (NPF Lumex AP) in the region 400–4000 cm^{-1} , with a resolution of 1 cm^{-1} . Samples were prepared as thin film in CH_2Cl_2 .

3.2. NMR Spectra

^1H , $^{13}\text{C}\{\text{H}\}$ and $^{11}\text{B}\{\text{H}\}$ NMR spectra of solutions of the studied substances in CD_3CN or CD_2Cl_2 were recorded on a Bruker MSL-300 pulsed Fourier spectrometer (Germany), at frequencies of 300.3, 75.49 and 96.32 MHz, respectively, with internal deuterium stabilisation. Tetramethylsilane or boron trifluoride ether was used as the external standard.

3.3. Electrospray Ionisation Mass Spectrometry (ESI-MS)

The LC system consisted of two LC-20AD pumps (Shimadzu, Japan) and an autosampler was coupled online with an LCMS-IT-TOF mass spectrometer equipped with an electrospray ionisation source (Shimadzu, Japan). The HRMS spectra were acquired in direct injection mode without column. The samples were prepared as CH_3CN solutions. Detection parameters: Detector Voltage 1.55 kV; Nebulising Gas 1.50 L/min; CDL Temperature 200.0 $^\circ\text{C}$.

3.4. X-ray Diffraction

The single-crystal X-ray diffraction data for 1 and 2 were collected using a three-circle Bruker D8 Venture (Centre of Joint Equipment of Kurnakov Institute of General and Inorganic Chemistry, Russian Academy of Sciences), in φ and ω scan mode. The data were indexed and integrated using the SAINT program [No Title. Bruker, SAINT, Bruker AXS Inc., Madison, WI, 2018.]. Absorption correction based on measurements of equivalent reflections (SADABS) was applied [53]. The structures were determined by direct methods and refined using the full-matrix least squares technique on F2 with anisotropic displacement parameters for non-hydrogen atoms. The hydrogen atoms in all compounds were placed in calculated positions and refined with the riding model with fixed isotropic displacement parameters [$U(\text{H}) = 1.5U(\text{C})$ for the CH_3 -groups and $1.2U(\text{C})$ for the other groups].

All calculations were carried out using the SHELXTL program [54] and OLEX2 program package [55]. For details, see Table S1 (Electronic Supporting Information).

The crystallographic data were deposited with the Cambridge Crystallographic Data Center, CCDC 2206019–2206020. Copies of this information may be obtained, free of charge, from the Director, CCDC, 12 Union Road, Cambridge CB2 1EZ, UK (Fax: +44 1223 336033; e-mail: deposit@ccdc.cam.ac.uk or www.ccdc.cam.ac.uk).

As it stated previously the crystals for X-ray diffraction experiments were obtained by isothermal evaporation of acetonitrile solutions of the corresponding derivative, in the presence of $(\text{C}_2\text{H}_5)_4\text{NCl}$ or $(\text{C}_6\text{H}_5)_4\text{PCl}$.

3.5. Hirshfeld Surface Analysis

The Crystal Explorer 17.5 program was [56] used to analyse the interactions within the crystal. The donor–acceptor groups were visualised using a standard (high) surface resolution and d_{norm} surfaces were mapped over a fixed colour scale of -0.640 (red) to 0.986 (blue) a.u.

3.6. Computational Details

DFT calculations were made using the ORCA 4.2.1 program package [57]. Geometries of all model structures were fully optimised at the $\omega\text{B97X-D3/def2-TZVPP}$ level of the-

ory [56,58]. All calculations were performed using the RIJCOSX approximation with the def2/J auxiliary basis set [59]. Tight criteria of SCF convergence (Tight SCF) were employed for the calculations. the keywords Grid5 FinalGrid6 GridX5 were used as parameters for the spatial integration grid All of the nitrilium derivatives considered had closed electron shells and the spin restricted approximation was applied. During the geometry optimisation procedure, symmetry operations were not applied for the structures considered. The Hessian matrices were calculated numerically for all model structures, to prove the location of correct minima on potential energy surfaces; (in all cases, no imaginary frequencies were found). Solvent effects were taken into account using the Solvation Model based on Density (SMD) [60]. The natural bond orbital (NBO) method (for calculation of Wiberg bond indices in Natural Atomic Orbitals) was employed using the NBO7 program package [61]. The Cartesian atomic coordinates for all optimised model structures of nitrilium derivatives of *closo*-dodecaborate anion are presented in the Supporting Information. The visualisation of optimised structures and their LUMO was performed with the help of the ChemCraft program (version 1.7) [62].

Solvents of reagent and special purity grades Sigma-Aldrich and Panreac (99.7%), were used without any additional purification.

3.7. Synthesis of Nitrilium Derivatives of the *closo*-Dodecaborate Anion $[B_{12}H_{11}NCR]^-$ $R=CH_3$, $n-C_3H_7$, $i-C_3H_7$, $4-C_6H_4CH_3$, $1-C_{10}H_7$

$((n-C_4H_9)_4N)[B_{12}H_{11}(NCCH_3)]$ (**1a**) was prepared by the known procedure [52]. 0.313 g (0.5 mmol) of $((n-C_4H_9)_4N)_2[B_{12}H_{12}]$ were dissolved in 10 mL of acetonitrile CH_3CN . The solution was placed in a glass pressure vessel, it was purged with argon and then 0.3 mL trifluoroacetic acid CF_3COOH was added. The reaction solution was heated to 150 °C. After 30 min of heating, the solution was cooled to room temperature and concentrated in a rotary evaporator. To this solution, 15 mL of glacial acetic acid CH_3COOH was added. The precipitate was filtered through a glass filter and washed with 30 mL glacial acetic acid and 30 mL diethyl ether. The product was dried in vacuo. Yield: 76%.

$((n-C_4H_9)_4N)[B_{12}H_{11}(NCn-C_3H_7)]$ **1b**

The method used was similar to **1a**. Yield: 73%. $^{11}B\{H\}$ NMR (ppm, CD_2Cl_2): -12.3 (s. 1B, B-N), -15.0 (s. 11B, B-H). 1H NMR (CD_2Cl_2 , ppm): 2.5–0.0 (m. 11H, B-H), 3.15 (8H, $(n-C_4H_9)_4N$), 1.61 (8H, $(n-C_4H_9)_4N$), 1.45 (8H, $(n-C_4H_9)_4N$), 1.01 (12H, $(n-C_4H_9)_4N$), 2.87 (t. 2H, $CH_2CH_2CH_3$, $J = 7.0$ Hz), 1.78 (m. 2H, $CH_2CH_2CH_3$), 1.03 (t. 3H, $CH_2CH_2CH_3$, $J = 7.4$ Hz). $^{13}C\{H\}$ NMR (CD_2Cl_2 , ppm): 59.4 ($(n-C_4H_9)_4N$), 24.4 ($(n-C_4H_9)_4N$), 20.2 ($(n-C_4H_9)_4N$), 13.9 (NBu4), 113.2 (NC- CH_3), 20.6 ($CH_2CH_2CH_3$), 18.9 ($CH_2CH_2CH_3$), 13.3 ($CH_2CH_2CH_3$). IR(CH_2Cl_2 , cm^{-1}): 2493 ν (B-H), 2338 ν (C \equiv N). MS(ESI) m/z : 210.2651 (A refers to the molecular weight of $[B_{12}H_{11}(NCn-C_3H_7)]$). Calculated for $\{[A]-\}$ 210.2629.

$((n-C_4H_9)_4N)[B_{12}H_{11}(NCi-C_3H_7)]$ **1c**

The method used was similar to **1a**. Yield: 69%. $^{11}B\{H\}$ NMR (CD_2Cl_2 , ppm): -12.0 (s. 1B, B-N), -15.2 (s. 11B, B-H). 1H NMR (ppm, CD_2Cl_2): 2.5–0.0 (m. 11H, B-H), 3.15 (8H, $(n-C_4H_9)_4N$), 1.61 (8H, $(n-C_4H_9)_4N$), 1.45 (8H, $(n-C_4H_9)_4N$), 1.01 (12H, $(n-C_4H_9)_4N$), 3.28 (m. 1H, $CH(CH_3)_2$, $J = 7.0$ Hz), 1.38 (d. 6H, $CH(CH_3)_2$, $J = 7.0$ Hz). $^{13}C\{H\}$ NMR (CD_2Cl_2 , ppm): 59.4 ($(n-C_4H_9)_4N$), 24.4 ($(n-C_4H_9)_4N$), 20.2 ($(n-C_4H_9)_4N$), 13.9 ($(n-C_4H_9)_4N$), 115.5 (NC- CH_3), 21.7 ($CH(CH_3)_2$), 18.3 ($H(CH_3)_2$), IR(CH_2Cl_2 , cm^{-1}): 2499 ν (B-H), 2338 ν (C \equiv N). MS(ESI) m/z : 210.2623 (A refers to the molecular weight of $[B_{12}H_{11}(NCi-C_3H_7)]$). Calculated for $\{[A]-\}$ 210.2629.

$((n-C_4H_9)_4N)[B_{12}H_{11}(NCC_6H_4CH_3)]$ **2a**

A mixture of 0.313 g (0.5 mmol) of $((n-C_4H_9)_4N)_2[B_{12}H_{12}]$, and 5 g of $NCC_6H_4CH_3$, was placed in an autoclave and then heated until melting in an argon stream. To the melt, 0.2 mL of CF_3COOH was added. The autoclave was heated to 150 °C and then kept for 30 min. The solution was cooled until crystallisation. The resulting solid mixture was transferred into a round-bottom flask and the excess nitrile was distilled off in a vacuum. The product obtained was dissolved in 5 mL of CH_3COOH/CF_3COOH mixture and left

for two hours. The resulting product was filtered off, washed with two portions of an acid mixture, 20 mL of cold diethyl ether, and dried in vacuo. The yield was 69%.

$^{11}\text{B}\{^1\text{H}\}$ NMR (ppm, CD_2Cl_2): -12.2 (s. 1B, B-N), -14.5 (s. 11B, B-H), ^1H NMR (CD_2Cl_2 , ppm): 2.5–0.0 (m. 11H, B-H), 3.16 (8H, (*n*- C_4H_9) $_4\text{N}$), 1.64 (8H, (*n*- C_4H_9) $_4\text{N}$), 1.43 (8H, (*n*- C_4H_9) $_4\text{N}$), 1.01 (12H, (*n*- C_4H_9) $_4\text{N}$), 7.76 (d. 2H, C_6H_4 $J = 7.9$ Hz), 7.43 (d. 2H, C_6H_4 $J = 8.1$ Hz), 2.49 (s. 3H, CH_3). $^{13}\text{C}\{^1\text{H}\}$ NMR (CD_2Cl_2 , ppm): 59.5 ((*n*- C_4H_9) $_4\text{N}$), 24.5 ((*n*- C_4H_9) $_4\text{N}$), 20.2 ((*n*- C_4H_9) $_4\text{N}$), 13.9 ((*n*- C_4H_9) $_4\text{N}$), 149.4, 134.3, 131.2 108.8 (C_6H_4), 103.3 ($\text{N}\equiv\text{C}$), 22.7 (CH_3). IR(CH_2Cl_2 , cm^{-1}): 2500 ν (B-H), 2305 ν ($\text{C}\equiv\text{N}$), 1600 ν ($\text{C}=\text{C}$). MS(ESI) m/z : 258.2666 (A refers to the molecular weight of $[\text{B}_{12}\text{H}_{11}(\text{NCC}_6\text{H}_4\text{CH}_3)]$). Calculated for $\{[\text{A}]\}$ 258.2629).

(*n*- C_4H_9) $_4\text{N}$][$\text{B}_{12}\text{H}_{11}(\text{NC}(\text{1-}\text{C}_{10}\text{H}_7))$] 2b

The method used was similar to 2a. Yield: 36 %.

$^{11}\text{B}\{^1\text{H}\}$ NMR (CD_3CN , ppm): -12.2 (s. 1B, B-N), -14.8 (s. 11B, B-H), ^1H NMR (CD_3CN , ppm): 2.5–0.0 (m. 11H, B-H), 3.05 (8H, (*n*- C_4H_9) $_4\text{N}$), 1.61 (8H, (*n*- C_4H_9) $_4\text{N}$), 1.34 (8H, (*n*- C_4H_9) $_4\text{N}$), 0.94 (12H, (*n*- C_4H_9) $_4\text{N}$), 8.5–7.5 (m. 7H, C_{10}H_7). $^{13}\text{C}\{^1\text{H}\}$ NMR (CD_3CN , ppm): 54.1 ((*n*- C_4H_9) $_4\text{N}$), 26.4 ((*n*- C_4H_9) $_4\text{N}$), 20.6 ((*n*- C_4H_9) $_4\text{N}$), 14.0 ((*n*- C_4H_9) $_4\text{N}$), 138.6, 137.6, 134.6, 134.1 133.8, 131.5, 130.7, 129.5, 126.5, 124.6 (C_{10}H_7), 104.2 ($\text{N}\equiv\text{C}$). IR(CH_2Cl_2 , cm^{-1}): 2502 ν (B-H), 2304 ν ($\text{C}\equiv\text{N}$), 1623, 1506 ν ($\text{C}=\text{C}$). MS(ESI) m/z : 294.2643 (A refers to the molecular weight of $[\text{B}_{12}\text{H}_{11}(\text{NCC}_{10}\text{H}_7)]$). Calculated for $\{[\text{A}]\}$ 294.2629).

4. Conclusions

The present work featured a complex investigation of nitrilium derivatives of *closo*-dodecaborate anion $[\text{B}_{12}\text{H}_{11}\text{NCR}]^-$, $\text{R} = n\text{-C}_3\text{H}_7$, *i*- C_3H_7 , 4- $\text{C}_6\text{H}_4\text{CH}_3$, 1- C_{10}H_7 . The range of nitrilium derivatives of *closo*-dodecaborate anions was expanded, including derivatives with *exo*-polyhedral substituents with aromatic backbones. The target derivatives could be obtained without complex purification procedures. All derivatives obtained were stable in air and could be stored without specific conditions (such as an argon atmosphere or vacuum conditions). Simplicity of purification and storage makes nitrilium derivatives of *closo*-dodecaborate anion $[\text{B}_{12}\text{H}_{11}\text{NCR}]^-$ promising as a starting platform for the formation of inorganic systems with various useful applications, including use in biomedicine. The increased reactivity of borylated nitriles in comparison with initial nitriles was explained with the help of DFT calculation. The carbon atom of the nitrilium group of $[\text{B}_{12}\text{H}_{11}\text{NCR}]^-$ became much more positively charged than the initial nitrile. This increase in positive charge also indicates that the carbon atom of the nitrilium group should be much more easily attacked by nucleophile molecules. In addition, the energies of the LUMO orbitals drastically change during the formation of the nitrilium complex. The decrease in LUMO energy during complex formation provides greater reactivity with nucleophile molecules.

Supplementary Materials: The following supporting information can be downloaded at: <https://www.mdpi.com/article/10.3390/inorganics10110196/s1>, Figure S1: $^{11}\text{B}\{^1\text{H}\}$ NMR spectrum (Bu_4N)[$\text{B}_{12}\text{H}_{11}(\text{NCnC}_3\text{H}_7)$] 1a; Figure S2: ^1H NMR spectrum (Bu_4N)[$\text{B}_{12}\text{H}_{11}(\text{NCnC}_3\text{H}_7)$] 1a; Figure S3: ^{13}C NMR spectrum (Bu_4N)[$\text{B}_{12}\text{H}_{11}(\text{NCnC}_3\text{H}_7)$] 1a; Figure S4: ESI-MS spectrum (Bu_4N)[$\text{B}_{12}\text{H}_{11}(\text{NCnC}_3\text{H}_7)$] (negative area) 1a; Figure S5: $^{11}\text{B}\{^1\text{H}\}$ NMR spectrum (Bu_4N)[$\text{B}_{12}\text{H}_{11}(\text{NCiC}_3\text{H}_7)$] 1b; Figure S6: ^1H NMR spectrum (Bu_4N)[$\text{B}_{12}\text{H}_{11}(\text{NCiC}_3\text{H}_7)$] 1b; Figure S7: ^{13}C NMR spectrum (Bu_4N)[$\text{B}_{12}\text{H}_{11}(\text{NCiC}_3\text{H}_7)$] 1b; Figure S8: ESI-MS spectrum (Bu_4N)[$\text{B}_{12}\text{H}_{11}(\text{NCiC}_3\text{H}_7)$] (negative area) 1b; Figure S9: $^{11}\text{B}\{^1\text{H}\}$ NMR spectrum (Bu_4N)[$\text{B}_{12}\text{H}_{11}(\text{NCC}_6\text{H}_4\text{CH}_3)$] 2a; Figure S10: ^1H NMR spectrum (Bu_4N)[$\text{B}_{12}\text{H}_{11}(\text{NCC}_6\text{H}_4\text{CH}_3)$] 2a; Figure S11: ^{13}C NMR spectrum (Bu_4N)[$\text{B}_{12}\text{H}_{11}(\text{NCC}_6\text{H}_4\text{CH}_3)$] 2a; Figure S12: ESI-MS spectrum (Bu_4N)[$\text{B}_{12}\text{H}_{11}(\text{NCC}_6\text{H}_4\text{CH}_3)$] (negative area) 2a; Figure S13: $^{11}\text{B}\{^1\text{H}\}$ NMR spectrum (Bu_4N)[$\text{B}_{12}\text{H}_{11}(\text{NCC}_{10}\text{H}_7)$] 2b; Figure S14: ^1H NMR spectrum (Bu_4N)[$\text{B}_{12}\text{H}_{11}(\text{NCC}_{10}\text{H}_7)$] 2b; Figure S15: ^{13}C NMR spectrum (Bu_4N)[$\text{B}_{12}\text{H}_{11}(\text{NCC}_{10}\text{H}_7)$] 2b; Figure S16: ESI-MS spectrum (Bu_4N)[$\text{B}_{12}\text{H}_{11}(\text{NCC}_{10}\text{H}_7)$] (negative area) 2b; Table S1 Cartesian atomic coordinates of the calculated optimized equilibrium model structures. All coordinates are given in Angstrom units. Optimized equilibrium model structures in gas phase; Table S2 Cartesian atomic coordinates of the calculated optimized equilibrium model structures. All coordinates are given in Angstrom units.

Optimized equilibrium model structures in dichloromethane; Table S3 Cartesian atomic coordinates of the calculated optimized equilibrium model structures. All coordinates are given in Angstrom units. Optimized equilibrium model structures in acetonitrile; Table S4 Crystal data and structure refinement for 1a and 1b.

Author Contributions: Manuscript conception, A.P.Z., I.N.K. and K.Y.Z.; writing and original draft preparation, A.V.N., I.N.K., A.S.N. and A.P.Z.; synthesis of derivatives A.V.N., A.P.Z., NMR analysis, N.A.S. and A.Y.B.; X-ray analysis, Hirshfeld analysis A.S.K.; quantum chemical calculations, I.N.K. and A.S.N.; editing, data analysis, and interpretation, A.P.Z., K.Y.Z. and N.T.K.; supervision, K.Y.Z. and N.T.K. All authors have read and agreed to the published version of the manuscript.

Funding: The work was supported by the Ministry of Science and Higher Education of the Russian Federation. Agreement No 075-15-2020-792, unique contract identifier RF—190220X0031.

Institutional Review Board Statement: Not applicable.

Informed Consent Statement: Not applicable.

Data Availability Statement: Not applicable.

Acknowledgments: A.S.N. is grateful to the RUDN University Strategic Academic Leadership Program.

Conflicts of Interest: The authors declare no conflict of interest.

References

1. Zhao, X.; Yang, Z.; Chen, H.; Wang, Z.; Zhou, X.; Zhang, H. Progress in Three-Dimensional Aromatic-like *Closo*-Dodecaborate. *Coord. Chem. Rev.* **2021**, *444*, 214042. [[CrossRef](#)]
2. Sivaev, I.B.; Bregadze, V.I.; Sjöberg, S. Chemistry of *Closo*-Dodecaborate Anion $[B_{12}H_{12}]_2^-$: A Review. *Collect. Czechoslov. Chem. Commun.* **2002**, *67*, 679–727. [[CrossRef](#)]
3. Ali, F.; Hosmane, N.S.; Zhu, Y. Boron Chemistry for Medical Applications. *Molecules* **2020**, *25*, 828. [[CrossRef](#)]
4. Golub, I.E.; Filippov, O.A.; Kulikova, V.A.; Belkova, N.V.; Epstein, L.M.; Shubina, E.S. Thermodynamic Hydricity of Small Borane Clusters and Polyhedral *Closo*-Boranes. *Molecules* **2020**, *25*, 2920. [[CrossRef](#)]
5. Tran, B.L.; Allen, T.N.; Bowden, M.E.; Autrey, T.; Jensen, C.M. Effects of Glymes on the Distribution of $Mg(B_{10}H_{10})$ and $Mg(B_{12}H_{12})$ from the Thermolysis of $Mg(Bh_4)_2$. *Inorganics* **2021**, *9*, 41. [[CrossRef](#)]
6. Lavallo, V.; Wright, J.H.; Tham, F.S.; Quinlivan, S. Perhalogenated Carba-*Closo*-Dodecaborate Anions as Ligand Substituents: Applications in Gold Catalysis. *Angew. Chem. Int. Ed.* **2013**, *52*, 3172–3176. [[CrossRef](#)]
7. Messina, M.S.; Axtell, J.C.; Wang, Y.; Chong, P.; Wixtrom, A.I.; Kirlikovali, K.O.; Upton, B.M.; Hunter, B.M.; Shafaat, O.S.; Khan, S.I.; et al. Visible-Light-Induced Olefin Activation Using 3D Aromatic Boron-Rich Cluster Photooxidants. *J. Am. Chem. Soc.* **2016**, *138*, 6952–6955. [[CrossRef](#)] [[PubMed](#)]
8. Zhao, X.; Yao, C.; Chen, H.; Fu, Y.; Xiang, C.; He, S.; Zhou, X.; Zhang, H. In Situ Nano Au Triggered by a Metal Boron Organic Polymer: Efficient Electrochemical N_2 Fixation to NH_3 under Ambient Conditions. *J. Mater. Chem. A* **2019**, *7*, 20945–20951. [[CrossRef](#)]
9. Avdeeva, V.V.; Malinina, E.A.; Kuznetsov, N.T. Boron Cluster Anions and Their Derivatives in Complexation Reactions. *Coord. Chem. Rev.* **2022**, *469*, 214636. [[CrossRef](#)]
10. Bolli, C.; Derendorf, J.; Jenne, C.; Scherer, H.; Sindlinger, C.P.; Wegener, B. Synthesis and Properties of the Weakly Coordinating Anion $[Me_3NB_{12}Cl_{11}]^-$. *Chem. A Eur. J.* **2014**, *20*, 13783–13792. [[CrossRef](#)]
11. Bolli, C.; Derendorf, J.; Jenne, C.; Keßler, M. Halogenated *Closo*-Dodecaborate Anions Stabilize Weakly Bound $[(Me_3NH)_3X]^{2+}$ ($X = Cl, Br$) Dications in the Solid State. *Eur. J. Inorg. Chem.* **2017**, *2017*, 4552–4558. [[CrossRef](#)]
12. Teprovich, J.A.; Colón-Mercado, H.; Washington II, A.L.; Ward, P.A.; Greenway, S.; Missimer, D.M.; Hartman, H.; Velten, J.; Christian, J.H.; Zidan, R. Bi-Functional $Li_2B_{12}H_{12}$ for Energy Storage and Conversion Applications: Solid-State Electrolyte and Luminescent down-Conversion Dye. *J. Mater. Chem. A* **2015**, *3*, 22853–22859. [[CrossRef](#)]
13. Duchêne, L.; Lünghammer, S.; Burankova, T.; Liao, W.-C.; Embs, J.P.; Copéret, C.; Wilkening, H.M.R.; Remhof, A.; Hagemann, H.; Battaglia, C. Ionic Conduction Mechanism in the $Na_2(B_{12}H_{12})_{0.5}(B_{10}H_{10})_{0.5}$ *Closo*-Borate Solid-State Electrolyte: Interplay of Disorder and Ion–Ion Interactions. *Chem. Mater.* **2019**, *31*, 3449–3460. [[CrossRef](#)]
14. Gigante, A.; Duchêne, L.; Moury, R.; Pupier, M.; Remhof, A.; Hagemann, H. Direct Solution-Based Synthesis of $Na_4(B_{12}H_{12})(B_{10}H_{10})$ Solid Electrolyte. *ChemSusChem* **2019**, *12*, 4832–4837. [[CrossRef](#)]
15. Hagemann, H. Boron Hydrogen Compounds: Hydrogen Storage and Battery Applications. *Molecules* **2021**, *26*, 7425. [[CrossRef](#)]
16. Barth, R.F.; Zhang, Z.; Liu, T. A Realistic Appraisal of Boron Neutron Capture Therapy as a Cancer Treatment Modality. *Cancer Commun.* **2018**, *38*, 36. [[CrossRef](#)]
17. Hattori, Y.; Kusaka, S.; Mukumoto, M.; Uehara, K.; Asano, T.; Suzuki, M.; Masunaga, S.; Ono, K.; Tanimori, S.; Kirihata, M. Biological Evaluation of Dodecaborate-Containing L-Amino Acids for Boron Neutron Capture Therapy. *J. Med. Chem.* **2012**, *55*, 6980–6984. [[CrossRef](#)]

18. Vaňková, E.; Lokočová, K.; Mařátková, O.; Křížová, I.; Masák, J.; Grüner, B.; Kaule, P.; Čermák, J.; Šícha, V. Cobalt Bis-Dicarbollide and Its Ammonium Derivatives Are Effective Antimicrobial and Antibiofilm Agents. *J. Organomet. Chem.* **2019**, *899*, 120891. [[CrossRef](#)]
19. Iguchi, Y.; Michiue, H.; Kitamatsu, M.; Hayashi, Y.; Takenaka, F.; Nishiki, T.; Matsui, H. Tumor-Specific Delivery of BSH-3R for Boron Neutron Capture Therapy and Positron Emission Tomography Imaging in a Mouse Brain Tumor Model. *Biomaterials* **2015**, *56*, 10–17. [[CrossRef](#)]
20. Avdeeva, V.V.; Garaev, T.M.; Breslav, N.V.; Burtseva, E.I.; Grebennikova, T.V.; Zhdanov, A.P.; Zhizhin, K.Y.; Malinina, E.A.; Kuznetsov, N.T. New Type of RNA Virus Replication Inhibitor Based on Decahydro-Closo-Decaborate Anion Containing Amino Acid Ester Pendant Group. *JBIC J. Biol. Inorg. Chem.* **2022**, *27*, 421–429. [[CrossRef](#)]
21. Sun, Y.; Zhang, J.; Zhang, Y.; Liu, J.; van der Veen, S.; Duttwyler, S. The Closo-Dodecaborate Dianion Fused with Oxazoles Provides 3D Diboraheterocycles with Selective Antimicrobial Activity. *Chem. A Eur. J.* **2018**, *24*, 10364–10371. [[CrossRef](#)] [[PubMed](#)]
22. Kusaka, S.; Hattori, Y.; Uehara, K.; Asano, T.; Tanimori, S.; Kirihata, M. Synthesis of Optically Active Dodecaborate-Containing l-Amino Acids for BNCT. *Appl. Radiat. Isot.* **2011**, *69*, 1768–1770. [[CrossRef](#)] [[PubMed](#)]
23. Knoth, W.H.; Sauer, J.C.; Miller, H.C.; Muetterties, E.L. Diazonium and Carbonyl Derivatives of Polyhedral Boranes. *J. Am. Chem. Soc.* **1964**, *86*, 115–116. [[CrossRef](#)]
24. Dou, D.; Mavunkal, I.J.; Bauer, J.A.K.; Knobler, C.B.; Hawthorne, M.F.; Shore, S.G. Synthesis and Structure of Triethylammonium 2-(Acetonitrile)Nonahydro-Closo-Decaborate(1-). *Inorg. Chem.* **1994**, *33*, 6432–6434. [[CrossRef](#)]
25. Mahfouz, N.; Ghaida, F.A.; El Hajj, Z.; Diab, M.; Floquet, S.; Mehdi, A.; Naoufal, D. Recent Achievements on Functionalization within Closo-Decahydrodecaborate $[B_{10}H_{10}]^{2-}$ Clusters. *ChemistrySelect* **2022**, *7*, e202200770. [[CrossRef](#)]
26. John, K.C.; Kaczmarczyk, A.; Soloway, A.H. Alkylation and Acylation of $B_{10}H_9NH_3^-$. *J. Med. Chem.* **1969**, *12*, 54–57. [[CrossRef](#)]
27. Grüner, B.; Bonnetot, B.; Mongeot, H. Synthesis of N- and B-Substituted Derivatives of Closo-Amino-Undecahydro-Dodecaborate(1-) Anion. *Collect. Czechoslov. Chem. Commun.* **1997**, *62*, 1185–1204. [[CrossRef](#)]
28. Koo, M.-S.; Ozawa, T.; Santos, R.A.; Lamborn, K.R.; Bollen, A.W.; Deen, D.F.; Kahl, S.B. Synthesis and Comparative Toxicology of a Series of Polyhedral Borane Anion-Substituted Tetraphenyl Porphyrins. *J. Med. Chem.* **2007**, *50*, 820–827. [[CrossRef](#)]
29. Sivaev, I.B.; Bruskin, A.B.; Nesterov, V.V.; Antipin, M.Y.; Bregadze, V.I.; Sjöberg, S. Synthesis of Schiff Bases Derived from the Ammoniaundecahydro-Closo-Dodecaborate(1-) Anion, $[B_{12}H_{11}NHCHR]^-$, and Their Reduction into Monosubstituted Amines $[B_{12}H_{11}NH_2CH_2R]^-$: A New Route to Water Soluble Agents for BNCT. *Inorg. Chem.* **1999**, *38*, 5887–5893. [[CrossRef](#)]
30. Zhang, Y.; Sun, Y.; Wang, T.; Liu, J.; Spingler, B.; Duttwyler, S. Synthesis and Structural Characterization of Amidine, Amide, Urea and Isocyanate Derivatives of the Amino-Closo-Dodecaborate Anion $[B_{12}H_{11}NH_3]^-$. *Molecules* **2018**, *23*, 3137. [[CrossRef](#)]
31. Stogniy, M.Y.; Erokhina, S.A.; Sivaev, I.B.; Bregadze, V.I. Nitrilium Derivatives of Polyhedral Boron Compounds (Boranes, Carboranes, Metallocarboranes): Synthesis and Reactivity. *Phosphorus Sulfur Silicon Relat. Elem.* **2019**, *194*, 983–988. [[CrossRef](#)]
32. Luzyanin, K.V.; Haukka, M.; Bokach, N.A.; Kuznetsov, M.L.; Kukushkin, V.Y.; Pombeiro, A.J.L. Platinum(IV)-Mediated Hydrolysis of Nitriles Giving Metal-Bound Iminols. *J. Chem. Soc. Dalt. Trans.* **2002**, *9*, 1882–1887. [[CrossRef](#)]
33. Kukushkin, V.Y.; Pombeiro, A.J.L. Additions to Metal-Activated Organonitriles. *Chem. Rev.* **2002**, *102*, 1771–1802. [[CrossRef](#)]
34. Zhdanov, A.P.; Klyukin, I.N.; Bykov, A.Y.; Grigoriev, M.S.; Zhizhin, K.Y.; Kuznetsov, N.T. Nucleophilic Addition of Alcohols to Anionic $[2-B_{10}H_9NCR]^-$ (R = Et, t-Bu): An Approach to Producing New Borylated Imidates. *Polyhedron* **2017**, *123*, 176–183. [[CrossRef](#)]
35. Bolotin, D.S.; Burianova, V.K.; Novikov, A.S.; Demakova, M.Y.; Pretorius, C.; Mokolokolo, P.P.; Roodt, A.; Bokach, N.A.; Suslonov, V.V.; Zhdanov, A.P.; et al. Nucleophilicity of Oximes Based upon Addition to a Nitrilium Closo-Decaborate Cluster. *Organometallics* **2016**, *35*, 3612–3623. [[CrossRef](#)]
36. Miller, H.C.; Hertler, W.R.; Muetterties, E.L.; Knoth, W.H.; Miller, N.E. Chemistry of Boranes. XXV. Synthesis and Chemistry of Base Derivatives of $B_{10}H_{10}^{2-}$ and $B_{12}H_{12}^{2-}$. *Inorg. Chem.* **1965**, *4*, 1216–1221. [[CrossRef](#)]
37. Zhizhin, K.Y.; Zhdanov, A.P.; Kuznetsov, N.T. Derivatives of Closo-Decaborate Anion $[B_{10}H_{10}]^{2-}$ with Exo-Polyhedral Substituents. *Russ. J. Inorg. Chem.* **2010**, *55*, 2089–2127. [[CrossRef](#)]
38. Nelyubin, A.V.; Klyukin, I.N.; Zhdanov, A.P.; Grigor'ev, M.S.; Zhizhin, K.Y.; Kuznetsov, N.T. Synthesis of Nitrile Derivatives of the Closo-Decaborate and Closo-Dodecaborate Anions $[B_nH_{n-1}NCR]^-$ (n = 10, 12) by a Microwave Method. *Russ. J. Inorg. Chem.* **2021**, *66*, 139–145. [[CrossRef](#)]
39. Voinova, V.V.; Selivanov, N.A.; Plyushchenko, I.V.; Vokuev, M.F.; Bykov, A.Y.; Klyukin, I.N.; Novikov, A.S.; Zhdanov, A.P.; Grigoriev, M.S.; Rodin, I.A.; et al. Fused 1,2-Diboraoxazoles Based on Closo-Decaborate Anion—Novel Members of Diboroheterocycle Class. *Molecules* **2021**, *26*, 248. [[CrossRef](#)]
40. Laskova, J.; Ananiev, I.; Kosenko, I.; Serdyukov, A.; Stogniy, M.; Sivaev, I.; Grin, M.; Semioshkin, A.; Bregadze, V.I. Nucleophilic Addition Reactions to Nitrilium Derivatives $[B_{12}H_{11}NCCCH_3]^-$ and $[B_{12}H_{11}NCCCH_2CH_3]^-$. Synthesis and Structures of Closo-Dodecaborate-Based Iminols, Amides and Amidines. *Dalt. Trans.* **2022**, *51*, 3051–3059. [[CrossRef](#)]
41. Šícha, V.; Plešek, J.; Kvíčalová, M.; Císařová, I.; Grüner, B. Boron(8) Substituted Nitrilium and Ammonium Derivatives, Versatile Cobalt Bis(1,2-Dicarbollide) Building Blocks for Synthetic Purposes. *Dalt. Trans.* **2009**, *5*, 851–860. [[CrossRef](#)] [[PubMed](#)]
42. Bogdanova, E.V.; Stogniy, M.Y.; Suponitsky, K.Y.; Sivaev, I.B.; Bregadze, V.I. Synthesis of Boronated Amidines by Addition of Amines to Nitrilium Derivative of Cobalt Bis(Dicarbollide). *Molecules* **2021**, *26*, 6544. [[CrossRef](#)] [[PubMed](#)]

43. Bogdanova, E.V.; Stogniy, M.Y.; Chekulaeva, L.A.; Anisimov, A.A.; Suponitsky, K.Y.; Sivaev, I.B.; Grin, M.A.; Mironov, A.F.; Bregadze, V.I. Synthesis and Reactivity of Propionitrilium Derivatives of Cobalt and Iron Bis(Dicarbollides). *New J. Chem.* **2020**, *44*, 15836–15848. [[CrossRef](#)]
44. El Anwar, S.; Růžičková, Z.; Baval, D.; Fojt, L.; Grüner, B. Tetrazole Ring Substitution at Carbon and Boron Sites of the Cobalt Bis(Dicarbollide) Ion Available via Dipolar Cycloadditions. *Inorg. Chem.* **2020**, *59*, 17430–17442. [[CrossRef](#)] [[PubMed](#)]
45. Stogniy, M.Y.; Erokhina, S.A.; Suponitsky, K.Y.; Anisimov, A.A.; Sivaev, I.B.; Bregadze, V.I. Nucleophilic Addition Reactions to the Ethylnitrilium Derivative of Nido-Carborane 10-EtCN-7,8-C₂B₉H₁₁. *New J. Chem.* **2018**, *42*, 17958–17967. [[CrossRef](#)]
46. Stogniy, M.Y.; Erokhina, S.A.; Suponitsky, K.Y.; Markov, V.Y.; Sivaev, I.B. Synthesis and Crystal Structures of Nickel(II) and Palladium(II) Complexes with *o*-Carboranyl Amidine Ligands. *Dalt. Trans.* **2021**, *50*, 4967–4975. [[CrossRef](#)] [[PubMed](#)]
47. Stogniy, M.Y.; Erokhina, S.A.; Anisimov, A.A.; Suponitsky, K.Y.; Sivaev, I.B.; Bregadze, V.I. 10-NCCH₂CH₂OCH₂CH₂C N-7,8-C₂B₉H₁₁: Synthesis and Reactions with Various Nucleophiles. *Polyhedron* **2019**, *174*, 114170. [[CrossRef](#)]
48. Stogniy, M.Y.; Bogdanova, E.V.; Anufriev, S.A.; Sivaev, I.B. Synthesis of New Rhodacarborane [3,3-(1',5'-COD)-8-PrNH=C(Et)NH-3,1,2-RhC₂B₉H₁₀]. *Russ. J. Inorg. Chem.* **2022**, *67*, 1537–1544. [[CrossRef](#)]
49. Calligaro, L.; Michelin, R.A.; Uguagliati, P. Mechanism of Nucleophilic Attack by Secondary Anilines on the Nitrile Group in Platinum(II) Ortho-Cyanobenzyl Complexes. *Inorg. Chim. Acta* **1983**, *76*, L83–L87. [[CrossRef](#)]
50. Uguagliati, P.; Belluco, U.; Michelin, R.A.; Guerriero, P. Reactions of Coordinated Nitriles. I. Mechanism of Formation of Amidino Complexes of Attack of Primary Anilines of Pt(II) Ortho-Cyanobenzyl Complexes. *Inorg. Chim. Acta* **1984**, *81*, 61–67. [[CrossRef](#)]
51. Ezhov, A.V.; Vyal'ba, F.Y.; Kluykin, I.N.; Zhdanova, K.A.; Bragina, N.A.; Zhdanov, A.P.; Zhizhin, K.Y.; Mironov, A.F.; Kuznetsov, N.T. Synthesis of New Bioinorganic Systems Based on Nitrilium Derivatives of *Closo*-Decaborate Anion and Meso-Arylporphyrins with Pendant Amino Groups. *Macrocyclics* **2017**, *10*, 505–509. [[CrossRef](#)]
52. Nelyubin, A.V.; Selivanov, N.A.; Bykov, A.Y.; Klyukin, I.N.; Novikov, A.S.; Zhdanov, A.P.; Karpechenko, N.Y.; Grigoriev, M.S.; Zhizhin, K.Y.; Kuznetsov, N.T. Primary Amine Nucleophilic Addition to Nitrilium *Closo*-Dodecaborate [B₁₂H₁₁NCCH₃][−]: A Simple and Effective Route to the New BNCT Drug Design. *Int. J. Mol. Sci.* **2021**, *22*, 13391. [[CrossRef](#)] [[PubMed](#)]
53. Krause, L.; Herbst-Irmer, R.; Sheldrick, G.M.; Stalke, D. Comparison of Silver and Molybdenum Microfocus X-Ray Sources for Single-Crystal Structure Determination. *J. Appl. Crystallogr.* **2015**, *48*, 3–10. [[CrossRef](#)] [[PubMed](#)]
54. Sheldrick, G.M. Crystal Structure Refinement with SHELXL. *Acta Crystallogr. Sect. C Struct. Chem.* **2015**, *71*, 3–8. [[CrossRef](#)]
55. Dolomanov, O.V.; Bourhis, L.J.; Gildea, R.J.; Howard, J.A.K.; Puschmann, H. OLEX2: A Complete Structure Solution, Refinement and Analysis Program. *J. Appl. Crystallogr.* **2009**, *42*, 339–341. [[CrossRef](#)]
56. Weigend, F.; Ahlrichs, R. Balanced Basis Sets of Split Valence, Triple Zeta Valence and Quadruple Zeta Valence Quality for H to Rn: Design and Assessment of Accuracy. Electronic Supplementary Information (ESI). *Phys. Chem. Chem. Phys.* **2005**, *7*, 3297–3305. [[CrossRef](#)]
57. Neese, F. The ORCA Program System. *WIREs Comput. Mol. Sci.* **2012**, *2*, 73–78. [[CrossRef](#)]
58. Grimme, S.; Antony, J.; Ehrlich, S.; Krieg, H. A Consistent and Accurate Ab Initio Parametrization of Density Functional Dispersion Correction (DFT-D) for the 94 Elements H-Pu. *J. Chem. Phys.* **2010**, *132*, 154104. [[CrossRef](#)]
59. Weigend, F. Accurate Coulomb-Fitting Basis Sets for H to Rn. *Phys. Chem. Chem. Phys.* **2006**, *8*, 1057–1065. [[CrossRef](#)]
60. Marenich, A.V.; Cramer, C.J.; Truhlar, D.G. Universal Solvation Model Based on Solute Electron Density and on a Continuum Model of the Solvent Defined by the Bulk Dielectric Constant and Atomic Surface Tensions. *J. Phys. Chem. B* **2009**, *113*, 6378–6396. [[CrossRef](#)]
61. Glendening, E.D.; Badenhoop, J.K.; Reed, A.E.; Carpenter, J.E.; Bohmann, J.A.; Morales, C.M.; Karafiloglou, P.; Landis, C.R.; Weinhold, F. *NBO 7.0: Natural Bond Orbital Analysis Program*; University of Wisconsin: Madison, WI, USA, 2018.
62. Chemcraft-Graphical Software for Visualization of Quantum Chemistry Computations. Available online: <https://www.chemcraftprog.com> (accessed on 16 September 2022).